Chapter 8

Multifractal Modeling and Analyses of Crustal Heterogeneity

David Marsan[1] and Christopher Bean[2]
[1]Laboratoire de Géophysique Interne et Tectonophysique, Université de Savoie, F-73376 Le Bourget du Lac, France; [2]Geology Department, University College Dublin, Belfield, Dublin 4, Ireland

1. INTRODUCTION

1.1 How heterogeneous is the upper crust?

Heterogeneity is a ubiquitous feature of both the sedimentary cover and the crystalline crust, present in most, if not all, physical properties. This is documented by borehole measurements of sonic velocities, neutron porosity, resistivity and many other physical properties. Borehole measurements provide the bulk of high-resolution data and have been exploited to demonstrate that small- to intermediate-scale variability, from centimeters to kilometers, is not simply random, uncorrelated noise. It is clear from such logs that variability is the norm and homogeneity the exception. As an example, Figure 1 shows the gamma log measured at the Cajon Pass borehole, exhibiting systematic fluctuations at all scales. Moreover, such variability is itself inhomogeneous (e.g., the variance at ~3200 m is greater than at ~2600 m). These measurements follow a heterogeneous, non-Gaussian distribution, with clusters of peaks departing from the mean well past the standard deviation.

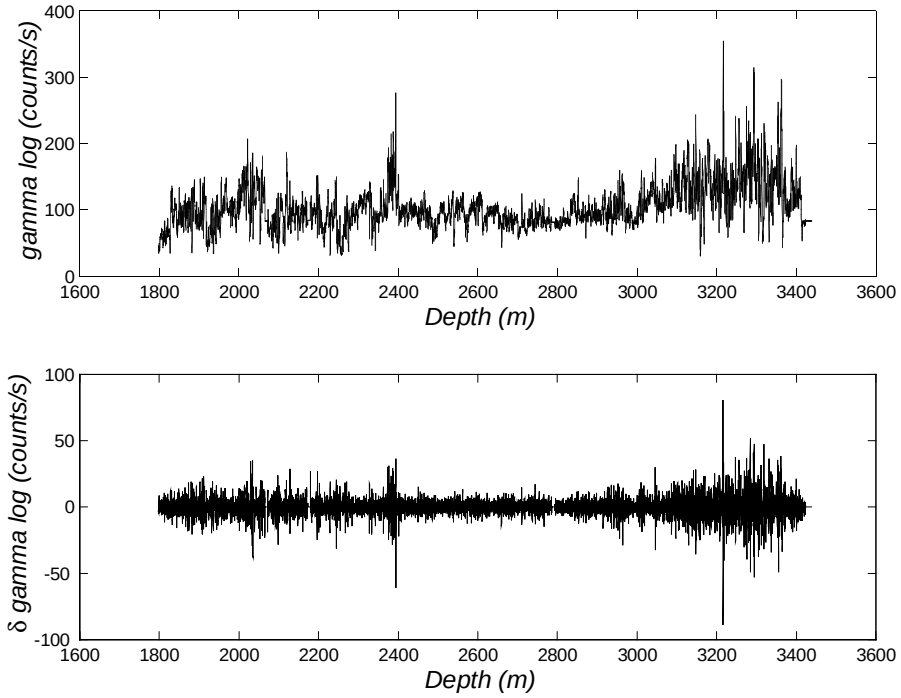

Figure 1. (Top) Gamma log from the Cajon Pass borehole, and (bottom) its derivative (sample-to-sample difference).

Scale-invariance is the absence of typical scales within a range of observation: a scale-invariant morphology appears (statistically) identical at all scales. Scale-invariance has been recognized as a robust statistical property, shared by many upper crustal medium characteristics. Numerous works have estimated fractal exponents of well logs (e.g., Todoeschuck *et al*., 1990; Bean and McCloskey, 1993; Wu *et al*., 1994; Holliger *et al*., 1996; Mehrabi *et al*., 1997; Dolan *et al*., 1998; and Leonardi and Kümpel, 1999). Power spectra of borehole sonic logs from many different locations and geologic settings display the ubiquitous $1/k$-decay, where k is the wavenumber. Scale-invariant fluctuations of the elastic parameters may be caused by fracture distributions (e.g., Leary, 1991, Holliger, 1996; Leary, this volume), lithologic variability (e.g., Bean, 1996; Goff and Holliger, 1999; Holliger and Goff, this volume), or porosity and fluid content. Such variability in material properties implies scale-invariant distributions of reflectors, and consequently a power law dependence of the scattering quality factor with frequency (Main *et al*., 1990) and an enrichment of the coda at high frequency (Leary, 1995). Coda waves are hence seen as direct

manifestations of the heterogeneous character of the medium in which the waves propagate.

The episodicity of the faulting/fracturing process, taking the form of strongly localized events, in both space and time, also shows the heterogeneity of both the stress and effective rheology of the medium. Deformation is localized to volumes much smaller than the loaded region, at least for mature enough systems. Furthermore, the redistribution of stress following the occurrence of a set of earthquakes with scale-invariant distribution of sizes, locations and times of occurrence is responsible for, and due to, scale-invariant, strongly heterogeneous stresses. The systematic occurrence and the complex character of aftershock sequences following a rupture event is symptomatic of how heterogeneous, but also how universal, the process of locally relaxing stress can be. Also, the activation and complex interactions between defects (quenched disorder) in a rock sample is known to diminish (by orders-of-magnitude) the strength of the sample subject to a fracturing experiment; small-scale heterogeneity plays a dominant role in the deformation process (a recent and rather extensive review of the role of defects in drastically reducing the strength of rocks can be found in Sornette, 2000; see also Herrmann and Roux, 1990).

Scale-invariant fluctuations of borehole breakout orientation with depth have been reported at the Cajon Pass borehole (Shamir and Zoback, 1992), suggesting that the classical view of a uniform regional stress driving the seismic activity of a fault zone is not only idealized, but likely to be inoperative and misleading. Crustal permeability is found to be highly heterogeneous, with fluctuations of several orders-of-magnitude and effectively infinite permeability gradients observed in both the crystalline crust (with, as proposed by Barton *et al*., 1995, most of the water transport accommodated by potentially active faults; see also Ito and Zoback, 2000) and sediments (Liu and Molz, 1997; Painter, this volume; Leary, this volume). The extent of this heterogeneity, along with a likely highly non-linear response to perturbations, is such that one can ask whether a systematic dynamical behavior can be observed in crustal fluid movements, as for example in the case of co- and post-seismic pore fluid pressure readjustment (e.g., Grecksch *et al*., 1999).

We derive from this suite of observations an image of a strongly heterogeneous crust, with medium properties fluctuating at many different scales. As briefly described here, such complexity is both due to and responsible for the complexity of crustal processes; tectonic deformation, fluid transport and seismic wave propagation are all found to exhibit complex and intricate behavior. Hence the study of such processes requires us to account for the heterogeneity of the medium. To neglect such heterogeneity, for example through deterministic modeling within a

homogeneous or slowly varying crust, is to ignore much of the character of such processes.

1.2 The multifractal model

The aim of this paper is to review one of the most advanced attempts at statistically characterizing crustal small-scale heterogeneity. By proposing increasingly realistic models and by studying their properties we hope to achieve a better understanding of how dynamical processes can develop within the crust. Multifractal distributions are scale-invariant, and as such can reproduce the power law scaling laws that are observed in borehole logs. Figure 2 shows several examples of power spectra $E(k)$ of various logs. Note that no obvious break of scaling is observed at large scales, where insufficient sampling can lead to spurious leveling-off, nor at small scale as long as the averaging effect of the tool is removed (Bean, 1996).

While the computation of the power spectrum is of great interest, allowing to test for the existence of a scaling law, it only gives limited information on how this signal needs to be statistically rescaled when zooming in or out. Mono-scaling characterizations typically lead to the estimate of the Hurst exponent H, such that $E(k) \sim k^{-1-2H}$. Characterizations of this type, either simple fractals or superposition of independent monofractal distributions (Goff and Holliger, 1999), are generally insufficient to accurately describe this rescaling. In particular, heterogeneity in the level of fluctuation and the intermittency of the signals cannot be retrieved by this method. For example in the case of the gamma log shown in Figure 1, the spatial variability in the variance could not be modeled with a monofractal analysis. These variations in the degree of "roughness" of the signal, and therefore of the local Hurst exponent, call for a modeling approach that allows for a location-dependent scaling exponent, itself distributed in a scale-invariant way (otherwise scale-invariance would be broken, as in the case of a modeling approach which adopts separate "units" of distinct monofractals).

Multifractal modeling was originally developed for the study of turbulent phenomena to account for and reproduce scale-invariant variations in the local level of fluctuations (in particular for the energy flux), and also for the characterization of strange attractors. The goal of this contribution is twofold: (1) to review previous analyses of multifractality for various crustal characteristics, such as borehole logs and fracture/fault patterns, and (2) to provide methods for numerically generating multifractal distributions with statistics that mimic the observed statistics of actual crustal quantities. This then allows for the numerical study of dynamical crustal processes with a realistic level of heterogeneity.

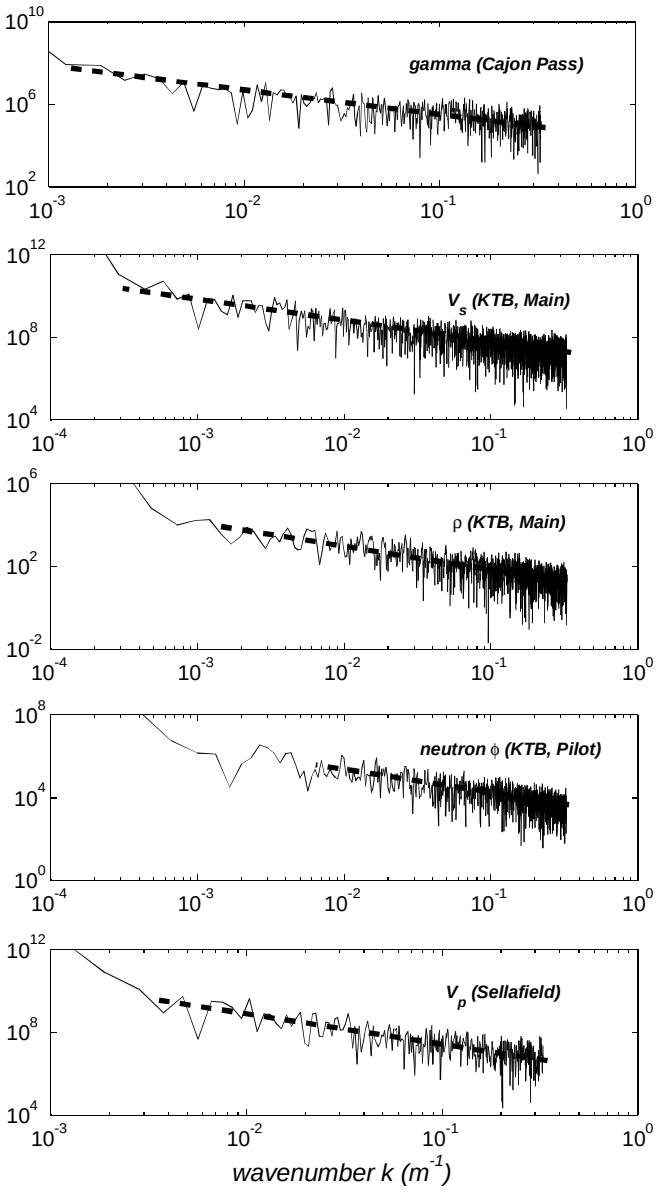

Figure 2. Power spectra of five logs from various boreholes, from top to bottom: a) gamma log from the Cajon Pass borehole; b) S-wave sonic log from the KTB main borehole, Germany; c) resistivity log from the KTB main borehole; d) neutron porosity log from the KTB pilot borehole (note the existence of two distinct scaling regimes with a transition at about 100m); e) P-wave sonic log from the Nirex 1 borehole at Sellafield, UK. The dashed black lines give power law fits $\sim k^{-\beta}$ of the spectrum decay, with spectral exponent β equal to a) 1.22, b) 0.98, c) 1.31, d) 1.37, and e) 1.4. All four boreholes probe the crystalline part of the upper crust.

In the following, we provide some basic theory of multifractal analysis and model construction. This is necessarily quite detailed mathematically, but only the properties and characteristics that are of primary importance to a geophysical modeler are discussed. Multifractals are mainly seen in this chapter as a way for modeling and reproducing the heterogeneity of the crust, especially as observed in well logs. This is, for example, of importance for the modeling of crustal transport phenomena, since extreme but rare values of permeability strongly control the flow regime. It is also important for wave propagation, since large fluctuations in the elastic parameters are what are primarily observed in seismic reflection data. This approach does not, however, propose a physical background for the emergence of this complexity (see Leary, this volume, and Holliger and Goff, this volume).

2. CONSTRUCTION AND PROPERTIES OF MULTIFRACTALS

This section details the construction and several important properties of multifractal distributions. It has been written for those who would like to get a deeper understanding of what multifractals are, but special attention has been paid to limiting the mathematical developments. As such, this section contains the minimum material that we think is required for someone wanting to numerically generate multifractal distributions. The Matlab® code given at the end of this chapter corresponds to the models developed in this section. Section 2.1.1 is the most directly accessible, while the other sections (in particular 2.3.1-3) can be skipped for a first reading.

2.1 Multiplicative cascade models

2.1.1 Construction and characterization

The generic construction of a multifractal distribution is given by multiplicative cascade models. These models are at the basis of all numerical methods for generating multifractal distributions, and hence need to be detailed. We first describe the simple 2-D case of a self-similar multifractal $\varepsilon_\ell(\underline{x})$, developed from an outer scale L down to the resolution scale ℓ; the maximum scale ratio is $\Lambda=L/\ell$. The notation ε classically refers to the turbulent energy flux, for which these models have originally been introduced (see Frisch, 1995, for a review). At scale ℓ, we expect to have Λ x Λ "structures", or "patches", within which ε is only slowly varying. The parameter ε_ℓ is therefore defined as a 2-D set, or field, of Λ^2 values. These

intensity values are obtained by fragmenting ε from the largest scale L down to ℓ, in a recursive, scale-invariant process (Figure 3): a structure at any intermediate scale l, with intensity $\varepsilon_l(\underline{x})$, is divided into four new, smaller structures $\varepsilon_{l/2}(\underline{x}_1),...,\varepsilon_{l/2}(\underline{x}_4)$ at scale $l/2$, with intensities equal to $\varepsilon_{l/2}(\underline{x}_i)=\varepsilon_l(\underline{x})\mu_i$. The μ_i are independent realizations of a unique positive random variable μ. The random value μ is only constrained by its non-negativity in the most general case. Additional constraints on μ arising from specific considerations will be discussed in Section 2.2. Scale-invariance of the process is ensured by applying this same step at all intermediate scales, starting with $\ell=L$, and drawing independent realizations of the same random variable μ at all scales. After n steps, ε is obtained at scale $L/2^n$; thus, $N=\log(L/\ell)/\log 2$ steps are required to generate ε_ℓ at scale ℓ. A multifractal distribution such as ε_ℓ is typically characterized by the scaling of its moments $<\varepsilon_\ell^q>$ with scale ℓ.

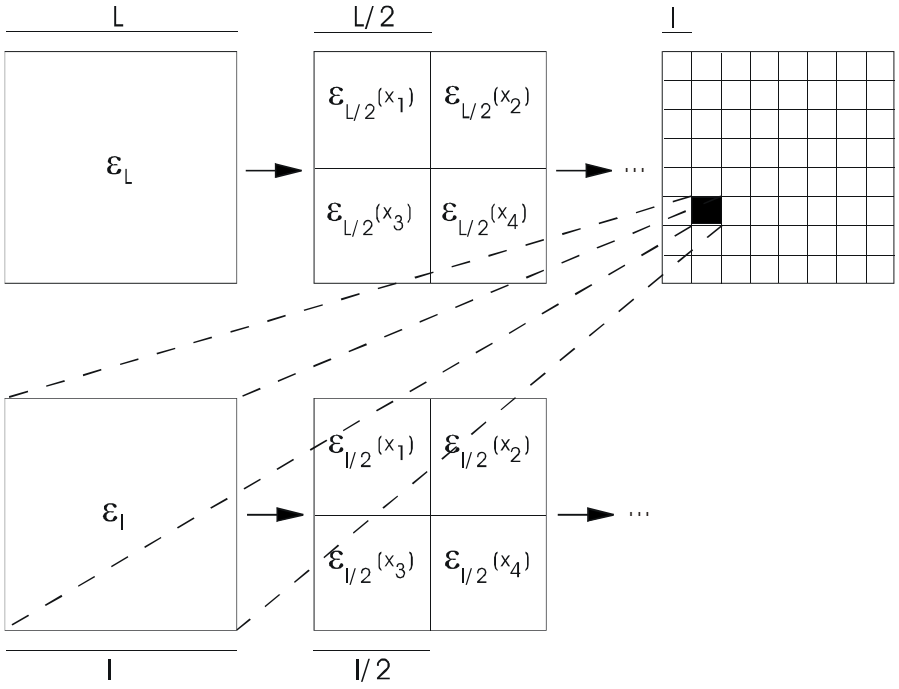

Figure 3. Construction of a multiplicative cascade with fragmentation of a "parent" structure into 2 x 2 new "children" structures. A child structure at scale $l/2$ is given a "weight" $\varepsilon_{l/2}$ equal to the weight ε_l of its parent times a realisation of the random variable μ.

The moment of order q of ε_ℓ is

$$<\varepsilon_\ell{}^q>=<(\varepsilon_L\mu^N)^q>=\varepsilon_L{}^q<\mu^q>^N, \qquad (1)$$

since the N realizations of μ are all independent of each other. The angled brackets indicate ensemble averaging. The moment scaling function $K(q)$ is effectively the second (Laplace) characteristic function of $\log\mu$. Denoting $K(q)=-\log<\mu^q>/\log 2$, we have $<\mu^q>=2^{-K(q)}$ and therefore

$$<\varepsilon_\ell{}^q> = \varepsilon_L{}^q \; 2^{-NK(q)} \sim \ell^{-K(q)}, \qquad (2)$$

where the symbol "~" denotes leading order variations with ℓ. So-called "conservative multifractals" (Mandelbrot, 1974) correspond to a construction where $<\mu>=1$, i.e., $K(1)=0$, and hence $<\varepsilon_\ell>\sim\ell^0$, implying that the mean of ε is conserved (on ensemble average) during the cascade. We consider the case in which ε is strictly conserved, so that in the construction described here $(\mu_1+\mu_2+\mu_3+\mu_4)/4=1$. As coined by Mandelbrot (1974) by referring to statistical mechanics, this yields a "micro-canonical" conservation, as opposed to the canonical conservation assumed throughout this chapter. The two models would differ when considering the properties of locally smoothed distributions (Schertzer and Lovejoy, 1987).

Equation (2) tells us that the moments of order q of the distribution scale with the scale of observation ℓ, and with an *a priori* arbitrary scaling exponent $K(q)$ specified by the choice of the random variable μ. The moment scaling function $K(q)$ is constrained by $K(1)=0$, since $<\mu>=1$, and $K(0)=0$, due to the normalization of the random variable μ, and its convexity. Strict convexity (i.e., $d^2K(q)/dq^2>0$) of $K(q)$ implies that, for $q_2>q_1$, $K(q_2)>K(q_1)q_2/q_1$, so that, as small scales $\ell\to 0$, the higher moments of the distribution grow more quickly than what would be obtained for a mono-scaling (hence a linear) $K(q)$, i.e., for which $d^2K(q)/dq^2=0$. This results in a stronger heterogeneity at small scales as compared to mono-scaling models, and corresponds to a level of fluctuations of $\varepsilon_\ell(\underline{x})$ varying with the location $\underline{x}$; the more curved $K(q)$ is (i.e., the larger $d^2K(q)/dq^2$), the stronger is the heterogeneity in the fluctuation level (i.e., the more "multifractal" ε).

Scaling of the moments of ε can be associated with the local scaling of ε, such that the probability density $\Pr(\varepsilon_\ell\sim\ell^{-\gamma})$ of having ε_ℓ locally scaling in $\ell^{-\gamma}$ is $\Pr(\varepsilon_\ell\sim\ell^{-\gamma})\sim\ell^{c(\gamma)}$. The parameter γ is the local order of singularity, and its probability density function $\Pr(\varepsilon_\ell\sim\ell^{-\gamma})$ scales with a scaling exponent $c(\gamma)$ corresponding to the co-dimension of its support (Schertzer and Lovejoy, 1987). The two descriptions, in terms of singularities or in terms of the moments of ε, are equivalent ($c(\gamma)$ and $K(q)$ are indeed dual by a Legendre transform; Parisi and Frisch, 1985) as they contain the same information, and every one of them fully characterize the scaling statistics of ε. However, the description in $K(q)$ is the one that is the most readily available to the analyst (wavelet analysis, however, can be used to directly estimate $c(\gamma)$; Arneodo *et al*., 1988), as will be detailed in Section 3.

A more widespread set of characteristic functions of ε is can be determined utilizing the measure (rather than the density ε_ℓ)

$$E_l(\underline{x}) = \int_{|\underline{x}'|<l} d\underline{x}'\, \varepsilon_\ell(\underline{x}-\underline{x}') . \tag{3}$$

We then define the function $\tau(q)$ (Halsey *et al*., 1986; Meneveau and Sreenivasan, 1987) as $<E_l^q>\sim l^{D+\tau(q)}$, where D is the dimension of the domain on which ε is defined (in the present 2-D construction, D=2). It is straightforward to show that $\tau(q)=(q\text{-}1)D-K(q)$. Equivalently, we can determine the generalized dimensions

$$D(q)=\frac{\tau(q)}{q-1}=D-\frac{K(q)}{q-1} \tag{4}$$

(Grassberger and Procaccia, 1983). The values $D(0)$, $D(1)$ and $D(2)$ are called the capacity, information and correlation dimensions, respectively. Also, one can introduce the singularity α and the function $f(\alpha)$ such that $N(E_l\sim l^{\alpha})\sim l^{-f(\alpha)}$, N giving the number of occurrences of the singularity α. We find that $\alpha=D\text{-}\gamma$, and $f(\alpha)=D\text{-}c(\gamma)$; i.e., all the quantities α, $f(\alpha)$ and $\tau(q)$ depend on the dimension of the domain D, while γ, $c(\gamma)$ and $K(q)$ do not. The latter are therefore invariant when reducing the dimensionality of the distribution (for example, taking 1-D sections of a 2-D distribution).

2.1.2 Correlations

The construction of ε using a multiplicative cascade constrains the two-point statistics of the distribution, and hence its correlations. Using a derivation originally proposed by Yaglom (1966), we find that $\varepsilon_\ell(\underline{x})$ and $\varepsilon_\ell(\underline{x}+\Delta\underline{x})$ will correspond to similar structures from scale L down to scale $|\Delta\underline{x}|$, and then to two independent branches of the cascade from $|\Delta\underline{x}|$ to ℓ. Hence $<\varepsilon(\underline{x}+\Delta\underline{x})\varepsilon(\underline{x})>\sim<\varepsilon_{|\Delta\underline{x}|}{}^2><\varepsilon_{\ell/|\Delta\underline{x}|}>^2$, and with $K(1)$=0 it follows that

$$<\varepsilon(\underline{x}+\Delta\underline{x})\varepsilon(\underline{x})>\sim|\Delta\underline{x}|^{-K(2)} . \tag{5}$$

This is equivalent to a power spectrum scaling as $E(k)\sim k^{-1+K(2)}$. Note that $K(2)>0$ since $K(0)=K(1)=0$ and $d^2K(q)/dq^2\geq 0$, hence $-1+K(2)>-1$ for conservative multifractals. However, typical borehole logs (Figure 2) possess a spectral slope $\beta>1$, implying that the construction given here cannot be used as such to describe those logs. We will demonstrate in Section 2.3 how to obtain multi-affine distributions, or "non-conservative"

multifractals, from conservative multifractals, and thus how to relax this constraint. Note also that the computation of the power spectrum only yields one value (at q=2) of the function $K(q)$, and is therefore insufficient for determining the complete scaling statistics of ε.

2.1.3 Self-affinity

The construction given here is for a self-similar (scaling isotropy) cascade, hence generating a self-similar multifractal distribution. In other words, zooming must be identical in all directions. Self-affinity (anisotropic scaling, hence anisotropic zooming) can also be achieved by dividing a parent structure into structures of different sizes along the different axes (e.g., Lovejoy *et al*., 1987). For example, a fragmentation into 2 x 3 rather than into 2 x 2 structures would generate a self-affine multifractal such that Eq. (2) would now read

$$< (T_\lambda \varepsilon_\ell)^q > \sim \lambda^{K(q)}, \tag{6}$$

where the operator T_λ contracts/dilates anisotropically the two directions x and y

$$T_\lambda (x, y) \to (\lambda^{-1} x, \lambda^{-1+h} y), \tag{7}$$

where h measures the departure from self-similarity. In the case of a fragmentation into 2 x 3 structures, one gets that h=log3/log2-1. The parameter h is only constrained by the condition h<1, i.e., T_λ effectively zooms in both x and y directions when λ>1. Correlations are now of the form

$$< \varepsilon(\underline{x} + \Delta\underline{x}) \varepsilon(\underline{x}) > \sim \left\| \Delta \underline{x} \right\|^{-K(2)}, \tag{8}$$

where ||•|| is a scale function such that

$$\left\| T_\lambda (x, y) \right\| = \lambda^{-1} \left\| (x, y) \right\| \tag{9}$$

(Marsan *et al*., 1996; Schertzer *et al*., 1997). Typically, "classical" power spectrum computation of a self-affine 2-D multifractal would yield two scaling regimes; a unique regime is recovered when properly accounting for the scaling anisotropy. Self-affinity can be expected to characterize the crust, as the vertical and the lateral directions are unlikely to behave similarly,

given geological stratification. Lovejoy *et al*. (2001) reviewed previous analyses, along with new ones, showing that the exponent *h* typically ranges between -1 and -2 in the crust. Finally, a more complete description of the departure from self-similarity for scale-invariant distributions, giving not only self-affine but also more involved cases, can be obtained by recognizing the fact that the operator T_λ forms a parametric group, hence allowing for scale-invariant rotations as well (Lovejoy and Schertzer, 1985).

2.2 Multifractal models

The scaling statistics of the multifractal distribution $\varepsilon_\ell(\underline{x})$ introduced in Section 2.1 are described by the moment scaling function $K(q)$, defined by the Laplace characteristic function of the random variable μ: $<\mu^q>=2^{-K(q)}$ in the self-similar cascade first introduced. Since μ is arbitrary (as long as $<\mu>=1$, so as to give a canonically conservative multifractal, and $\mu \geq 0$), these statistics are thus also arbitrary, with only the few constraints on $K(q)$ already evoked in Section 2.1. Various theories and cascade models have been proposed over the past 50 years to fit empirically estimated $K(q)$ functions, especially for turbulent energy fluxes (or, rather, the non-conservative turbulent velocity fluctuations that are readily measurable). For such fluxes, the reproducibility of $K(q)$ is a remarkable feature, implying the existence of a fundamental mechanism responsible for it.

An important constraint on $K(q)$ can be formulated by recognizing that the fixed scale ratio λ_1, used to infer the scale l/λ_1 of a child structure from the scale l of its parent structure, is arbitrary. In Section 2.1, the self-similar cascade was constructed assuming $\lambda_1=2$, while other values of λ_1 can equally well be chosen, in which case the total number of steps N required to generate scale ℓ from L varies as $\lambda_1^N=L/\ell$. As an example, the multifractal statistics of a multifractal distribution ε_ℓ generated using $\lambda_1=2$ or $\lambda_1=3$ would then be identical if one assumes that, for a given set of L, ℓ and $K(q)$:

- case $\lambda_1=2$: $\log(L/\ell)/\log 2$, and $\mu_{(2)}$ (where the subscript denotes the scale ratio dependence) is such that $<\mu_{(2)}^q> = 2^{-K(q)}$;
- case $\lambda_1=3$: $\log(L/\ell)/\log 3$ and $<\mu_{(3)}^q> = 3^{-K(q)}$.

The construction described so far, assuming a given value for λ_1, is one of a discrete scale-invariant distribution; the cascade is only developed onto a discrete, and arbitrary, set of scales L, L/λ_1, L/λ_1^2,...,$L/\lambda_1^N=\ell$. Some authors have identified this discrete symmetry as an actual property of scale-invariant systems/distributions observed in nature, which could be responsible for log-periodic oscillations with period $\log\lambda_1$ in the dynamics of such systems (Huang *et al*., 1998; see Sornette and Sammis, 1995, and

Newman *et al*., 1995, for discussions on log-periodic dynamics). However, the question still arises as to why a preferred scale ratio λ_1 would be singled out or, equivalently, as to what constrains the set of favored scales to its a priori arbitrary state. This constraint can be relaxed by allowing a Poisson distribution of cascade steps constrained only by the average number of steps (She and Leveque, 1994). For our construction, this would imply fixing only a mean density of steps per scale ratio, hence a mean $\overline{\lambda_1}$. Writing

$$\overline{N} = \frac{\log L/\ell}{\log \overline{\lambda_1}}, \tag{10}$$

a Poisson distribution with mean density of cascade steps $\overline{\lambda_1}$ and $<\mu^q>=(\overline{\lambda_1})^{-K(q)}$ leads to a multifractal distribution with $<\varepsilon_\ell^q>\sim\ell^{-K(q)}$. The log-Poisson model of She and Leveque (1994) also assumes, for the turbulent energy flux, that μ is binomial; i.e., it can only take two (arbitrary) values.

The statistics of μ, and hence $K(q)$, can be constrained by noting that, when there is no privileged scale ratio λ_1, one can develop a cascade $\varepsilon_L \rightarrow \varepsilon_{L/\lambda}$ on any given scale ratio λ by choosing any real-valued $\lambda_1>1$ such that the increment $\mu_{(\lambda_1)}$ is, with the equality holding here for the distributions, $\mu_{(\lambda_1)^N} = \mu_{(\lambda)}$, where $\lambda=\lambda_1^N$, and therefore

$$\forall N, \quad N \log \mu_{(\lambda_1=\lambda^{1/N})} = \log \mu_{(\lambda)}. \tag{11}$$

The function $\log \mu_\lambda$ is therefore infinitely divisible (hence μ is log-infinitely divisible) (She and Waymire, 1995; Schertzer *et al*., 1995). This puts a strong constraint on μ, and consequently on the only acceptable $K(q)$ functions, limiting the choice to log-compound Poisson processes, for example: log-Gamma, log-Poisson, or log-Lévy statistics (Schertzer *et al*., 1995; Pocheau, 1998). Note that the scale densification $\lambda_1 \rightarrow 1$ of Schertzer and Lovejoy (1987) is equivalent to constraining μ to be log-infinitely divisible. The construction of continuous scale-invariant distributions is given in Schmitt and Marsan (2001) and takes a simple form owing to the stable nature of the model when considering log-Lévy statistics for μ (Schertzer and Lovejoy, 1987; Schmitt and Marsan, 2001). The property of attraction of Lévy-stable laws in regard to addition implies that they probe a domain of the phase space not only limited to just one point, unlike other infinitely divisible but non-stable distributions. Hence, the lognormal and, more generally, the log-Lévy statistics are somewhat expected to be more

commonly observed (one needs less constraints on the model to get them) than their non-stable counterparts. Figure 4 shows two examples of 2-D conservative lognormal multifractals, obtained from continuous ($\lambda_1 \to 1$) and discrete ($\lambda_1=2$) multiplicative cascades.

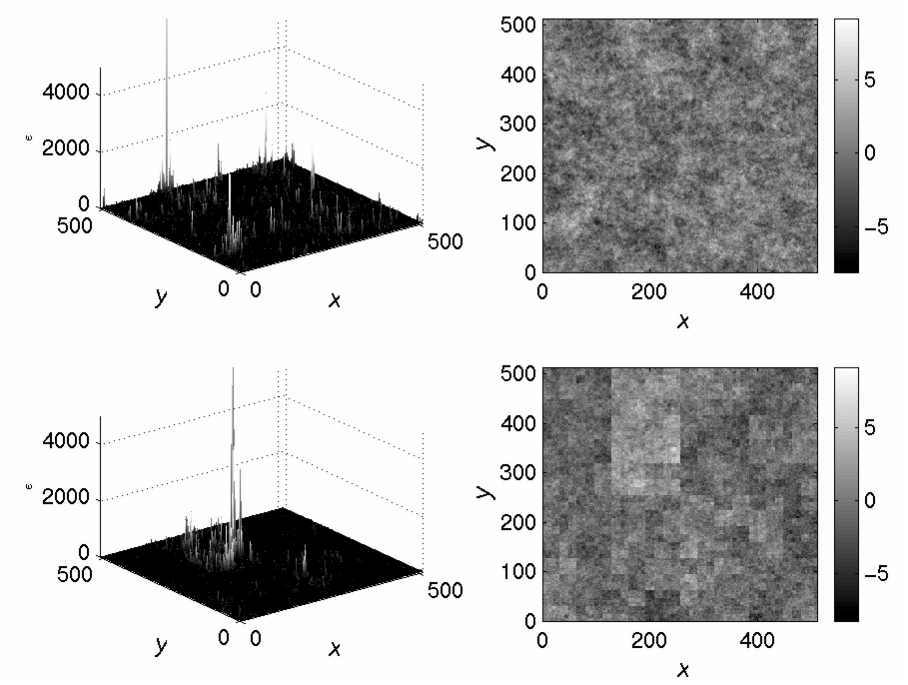

Figure 4. Two instances of a 2-D conservative lognormal multifractal, such that $K(q)=0.18(q^2-q)$. (Left) 3-D view of the distributions, (right) 2-D map view of their logarithms. (Top) Using a continuous cascade model, and (bottom) using a discrete ($\lambda_1=2$) cascade model. The structure with apparent squares of the latter is a direct consequence of the existence of a discrete set of scales on which the cascade is developed, while the continuous construction does not let such structures appear, by developing the cascade on a continuum of scales.

2.3 Non-conservative multifractal distributions

As remarked previously in Section 2.1, the multiplicative cascade model only generates conservative multifractals, such that the spectral slope β of the power spectrum $E(k) \sim k^{-\beta}$ is $\beta<1$. This is an overly constrictive limitation, since most borehole logs exhibit spectral slopes $\beta>1$ (e.g., Figure 2), and are therefore examples of non-conservative multifractal (Schertzer and Lovejoy, 1987), multi-affine (Vicsek and Barabási, 1991), or non-stationary multifractal (Davis *et al*., 1994) distributions. Several models, all elaborating on the multiplicative cascade model, have been shown to

generate multi-affine distributions: middle-point methods (Vicsek and Barabási, 1991), wavelet dyadic cascades (Benzi *et al*., 1993a; Arneodo *et al*., 1998), fractional integration of conservative multifractals (Schertzer and Lovejoy, 1987), and multifractal operational time processes (Mandelbrot, 1997). Denoting by $v(\underline{x})$ a multi-affine distribution, its scaling statistics can be detailed by examining the multi-scaling of its increments

$$<|v(x+\Delta x)-v(x)|^q>\sim|\Delta x|^{\zeta(q)}, \qquad (12)$$

where $\zeta(q)$ is called the structure function. Simple affine distributions, like fractional Brownian motions (Mandelbrot and Van Ness, 1968) or fractional Lévy motions (Taqqu, 1987) and their extension to D-dimensional domains are such that $\zeta(q)=Hq$, where H is the Hurst exponent. Note that for fractional Lévy motions, divergence of moments $q\geq\alpha$, where α is the Lévy index of the motion, leads to a bi-linear numerical $\zeta(q)$ (e.g., Schmitt *et al*., 1999; Nakao, 2000).

For multi-affine distributions, $\zeta(q)$ is no longer linear, and therefore, as for conservative multifractals, one needs more than just a single exponent to fully characterize their scale-invariant statistics. Note that the power spectrum $E_v(k)$ of v scales as $E_v(k)\sim k^{-1-\zeta(2)}$, and $\zeta(2)>0$ ensures that the spectral slope β such that $E_v(k)\sim k^{-\beta}$ is larger than 1. We here briefly recall two of the afore mentioned models, along with a third model, as candidates for easy-implementation computational routines for synthetic modeling purposes. Matlab® codes for such methods are given in the Appendix.

2.3.1 Multifractal operational time

The construction of a 1-D multi-affine distribution $v(t)$ can be given in terms of a compound fractional Brownian motion $w(\tau)$ with a multifractal operational time $\tau(t)$ such that

$$\tau(t)=\int_0^t dt'\,\varepsilon(t'), \qquad (13)$$

with ε being a conservative multifractal distribution (see Section 2.1), with $<\varepsilon_\ell^q>\sim\ell^{-K(q)}$. As shown by Mandelbrot (1997), the increments of $v(t)=w(\tau(t))$ scale like $<|v(t+\Delta t)-v(t)|^q>=<|w(\tau(t+\Delta t))-w(\tau(t))|^q>\sim<[\tau(t+\Delta t)-\tau(t)]^{qH}>$, H being the Hurst exponent of w. Hence we obtain

$$<\left|v(t+\Delta t)-v(t)\right|^q>\sim<\left[\int_t^{t+\Delta t}dt'\,\varepsilon(t')\right]^{qH}>\sim<\left[\Delta t\,\varepsilon_{\Delta t}\right]^{qH}>, \qquad (14)$$

and therefore $\langle|v(t+\Delta t)-v(t)|^q\rangle \sim \Delta t^{\zeta(q)}$ with $\zeta(q)=qH-K(qH)$. We can transform a mono-scaling process (e.g., a fractional Brownian motion) w into a multi-scaling process by properly mapping the 1-D domain $t \rightarrow \tau(t)$. The one-to-one mapping τ needs to be scale-invariant (the converse would imply distinguishing a set of characteristic scales for τ, which would then also emerge for v), continuous (so that no overlap nor gap is allowed), and non homogeneous, i.e., multifractal. Figure 5 shows an example of such a construction; v does indeed possess the scaling symmetry and heterogeneous structure characteristic of multifractal distributions.

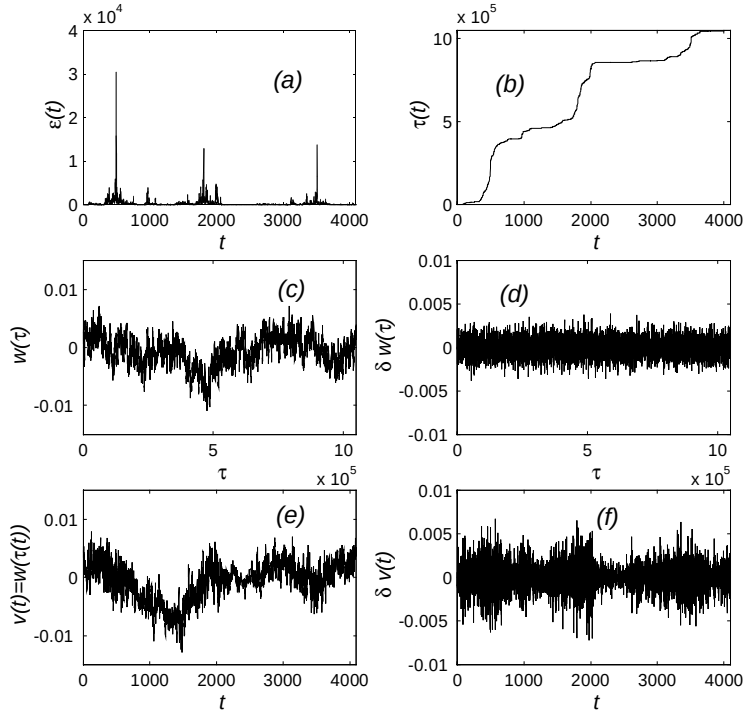

Figure 5. Construction of a 1-D, non-conservative multifractal $v(t)$ using the multifractal operational time method. a) A lognormal conservative multifractal $\varepsilon(t)$ with $K(q)=0.3(q^2-q)$ is generated using a continuous multiplicative cascade, and b) the operational time $\tau(t)$ is defined as the cumulative sum of $\varepsilon(t)$. c) A fractional Brownian motion $w(t)$ is computed with a Hurst exponent $H=0.1$, and e) the composition of w with τ yields the multi-affine $v(t)=w(\tau(t))$. d) and f) compare the derivatives of w and v, respectively, showing that the composition transforms an "homogeneous" fractal signal into an heterogeneous one with varying level of fluctuation. The structure function of $v(t)$ is $\zeta(q)=0.13q-0.003q^2$.

Extension of this method to (D>1)-dimensional domains is nontrivial; this would imply mapping vectors $d\underline{x}$ into $d\underline{x} \rightarrow d\underline{u}$ with $du = \underline{\underline{\varepsilon}}\, d\underline{x}$, and with the scaling condition on the "strain" $\underline{\underline{\varepsilon}}$ that

$$< \left\| \underline{\underline{\varepsilon}}\, d\underline{x} \right\|^q > \sim \left\| d\underline{x} \right\|^{q-K(q)} \tag{15}$$

in the general non-self similar case (ε is not symmetric, as it also accounts for possible rotations). The tensor field $\underline{\underline{\varepsilon}}$ needs to also verify the classical equations of compatibility. As far as we are aware, this type of construction has yet to be examined. Note that the form of the latter equation is generic to a multifractal tensorial distribution, and might therefore be thought of as being representative of the scaling symmetry prevailing for both the stress and the strain in the crust.

2.3.2 Fractional integration of $\varepsilon_\ell(\underline{x})$

A simple model for generating multi-affine distributions was proposed in Schertzer and Lovejoy (1987) and corresponds to directly changing the spectral slope β of a conservative multifractal $\varepsilon_\ell(\underline{x})$ by fractionally integrating it

$$v(\underline{x}) = \int d\underline{x}' \varepsilon_\ell(\underline{x}') \left| \underline{x} - \underline{x}' \right|^{-D+\chi}, \tag{16}$$

where D is the dimension of the domain, and χ is a parameter that is adjusted accordingly to the required spectral slope of v. Such a method can easily be implemented for any value of D. The Matlab® code given in the Appendix allows for the construction of 1-D and 2-D models. Note that only this method (unlike in Sections 2.3.1 and 2.3.3) can handle 2-D or 3-D simulations. This integration is similar to the construction of a fractional Brownian motion field, but acts on a multifractal measure rather than on a Gaussian "white noise". One can show (Schertzer *et al.*, 1997) that $v(\underline{x})$ verifies Eq. (12) with $\zeta(q)=\chi q - K(q)$, in the self-similar case. For a self-affine distribution, one needs to fractionally integrate over a self-affine $\varepsilon_\ell(\underline{x})$, i.e.,

$$v(\underline{x}) = \int d\underline{x}' \varepsilon_\ell(\underline{x}') \left\| \underline{x} - \underline{x}' \right\|^{-D_{el}+\chi}, \tag{17}$$

where D_{el} is the so-called elliptical dimension characteristic of the symmetry (e.g., Lovejoy *et al.*, 1987). In the self-affine construction given in Section 2.1 (where one structure divides into 2 x 3 structures and hence

$T_\lambda(x,y)\rightarrow(\lambda^{-1}x,\lambda^{-1+h}y)$ with h=log3/log2-1) this elliptical dimension is D_{el}=1+(1-h)=3-log3/log2=1.415 and Eq. (12) now reads

$$<\left|v(\underline{x}+\Delta\underline{x})-v(\underline{x})\right|^q>\sim\left\|\Delta\underline{x}\right\|^{\zeta(q)}, \text{ with } \left\|T_\lambda\,\underline{x}\right\|=\lambda^{-1}\left\|\underline{x}\right\|. \qquad (18)$$

While this method correctly generates the expected multi-affine distribution, it is unfortunately characterized by profiles with visual aspects that can differ from actual borehole logs. This comes from the fact that we fractionally integrate over a positive distribution $\varepsilon_\ell(\underline{x})$, hence a positive $v(\underline{x})$ with large fluctuations systematically characterized by positive onsets. However, this characteristic feature is sometimes observed for real logs, for which this method can therefore be exploited. We show in Figure 6 an example of such a construction that reproduces the multi-scaling statistics of the neutron porosity $\phi(z)$ of the KTB main borehole.

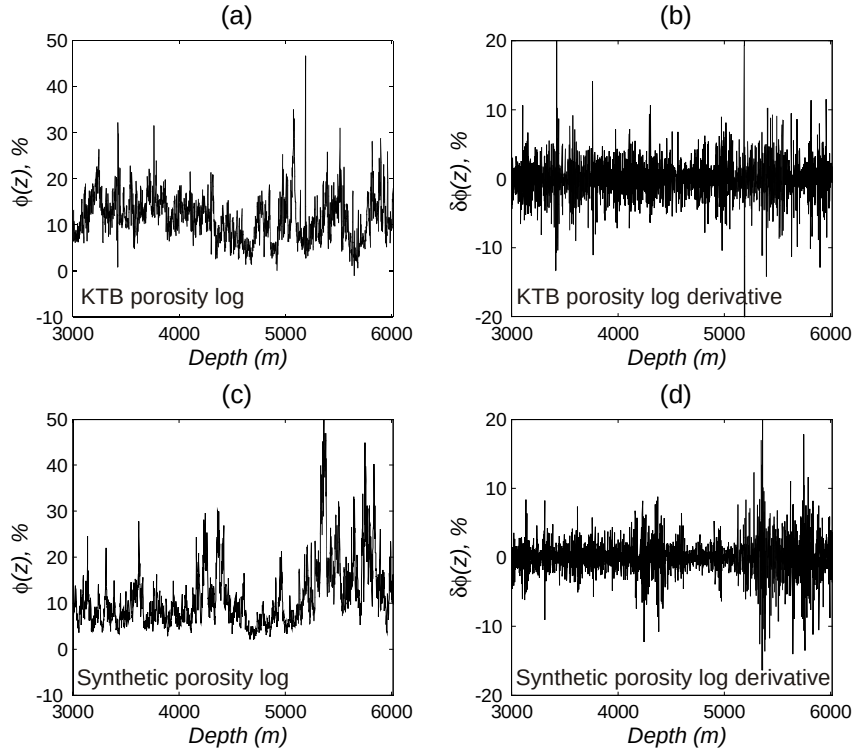

Figure 6. Modeling of a non-conservative multifractal signal: the case of the neutron porosity, $\phi(z)$, of the KTB Main borehole a) and its derivative b). The synthetic log c) is obtained by fractional integration of a continuous multiplicative cascade, and exhibit the same type of fluctuations for its derivative d) as those of the real signal b).

2.3.3 Two-step integration of a signed multifractal noise

A third method generates in three steps 1-D multi-affine distributions that closely mimic both the multi-scaling statistics and the overall characteristics of, for example, sonic and density logs. Starting from a conservative multifractal $\varepsilon(z)$ with moment scaling function $K(q)$, one can define increments $v(z+\Delta z)-v(z)$ by summing $\varepsilon^{1/2}(z)$ weighted by a Gaussian white noise $W(z)$ over the interval $z \rightarrow z+\Delta z$

$$v(z+\Delta z)-v(z)=\int_{z}^{z+\Delta z} dz'\varepsilon^{1/2}(z')W(z') \,. \tag{19}$$

This implies the scaling of the increments in

$$<\left|v(z+\Delta z)-v(z)\right|^{q}>=<\left|\int_{z}^{z+\Delta z} dz'\varepsilon(z')\right|^{q/2}>\sim \Delta z^{q/2-K(q/2)} \tag{20}$$

A final fractional integration/derivation can then be performed in order to adjust the spectral slope (hence the linear term of the structure function) as the spectral slope β of the process v given by the increments defined above is $\beta=2$. An example is shown in Figure 7.

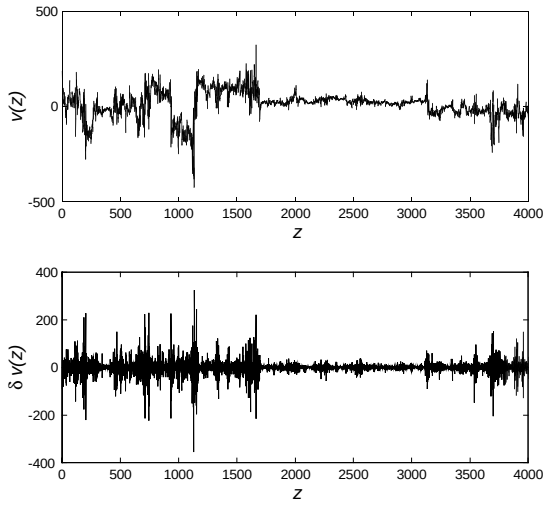

Figure 7. An instance of a non-conservative multifractal $v(z)$ (top), along with its derivative (bottom), obtained by the two-step integration method, starting from a lognormal conservative multifractal generated by a continuous multiplicative cascade. The structure function of $v(z)$ is $\zeta(q)=0.2q-0.05q^2$. The axes have arbitrary units.

3. MULTIFRACTAL ANALYSES OF BOREHOLE LOGS AND FRACTURE PATTERNS

Borehole logs provide detailed and reliable measurements of the geophysical state of the upper crust at depths of the order of one to a several kilometers. For example, the derivative of the P-wave sonic log gives a proxy of the reflectivity at the resolution scale, and is hence of great interest for examining the characteristics of the medium with regard to the scattering of seismic waves. We will in this section mainly report previous multifractal analyses of borehole logs. Also, a fundamental source of heterogeneity in the upper crust arises from fracture and fault patterns, and we will accordingly review attempts at analyzing and modeling multifractal distributions of fracture characteristics (location, length, cumulative displacement, aperture).

3.1 Analyses of borehole logs

Multifractal analyses of micro-resistivity (Saucier and Muller, 1993; Muller, 1993; Saucier *et al*., 1997), porosity (Muller, 1992), sonic (Herrmann, 1997, 1998; Marsan and Bean, 1999), and gamma (Marsan and Bean, 1999) logs have shown how one can quantify the multi-scaling statistics of crustal heterogeneities. Different techniques were employed to analyze such signals: direct structure function estimation through the scaling of the moments of the increments (Marsan and Bean, 1999), transformation of the signal by taking an (arbitrary) moment ω of the absolute value of the derivative (Saucier *et al*., 1997), or wavelet analysis (Herrmann, 1997, 1998). One aspect of these analyses, particularly in the case of Saucier and Muller (1993), Saucier *et al*. (1997), Muller (1992), and Marsan and Bean (1999), is that the scaling is either found to be restricted to rather short scale ranges (e.g., less than one decade in the case of Saucier and Muller, 1993) or of average quality, even though the associated power spectra display scaling regimes over several decades of scales. Such limitations are mainly due to the restricted number of data points, a particularly severe problem in most borehole log analysis as a maximum scaling range extending from 1 m to a few 100's of meters is typically the best which can be obtained with sufficient statistical convergence, after removal of the system response of the tool. Use of a method proposed by Benzi *et al*. (1993b) in the framework of extended-self-similarity (ESS), and developed for the study of turbulence, can improve the quality of the fit. Rather than a direct estimation of the scaling of increments $<|v_\ell(x+\Delta x)-v_\ell(x)|^q>$ with Δx, one can look at the scaling of one moment versus another

$$< \left| v_\ell(x+\Delta x) - v_\ell(x) \right|^{q_1} > \sim < \left| v_\ell(x+\Delta x) - v_\ell(x) \right|^{q_2} >^{\varsigma(q_1)/\varsigma(q_2)} . \qquad (21)$$

We then define $\tilde{\varsigma}(q) = \varsigma(q)/\varsigma(q^*)$, where q^* is an arbitrary moment, which can be taken to be equal to 2. This allows us to use the spectral slope of v, β, to fully constrain $\zeta(q)$: $\beta+1=\zeta(2)$, hence $\varsigma(q) = \tilde{\varsigma}(q)(\beta - 1)$. An advantage of this method is that it automatically accounts for the transition scales and multiple scaling regimes that could artificially arise from analyzing 1-D or 2-D slices of non-self-similar 3-D distributions (e.g., Schertzer *et al*., 1997).

The wavelet transform maxima modulus (WTMM) method (Muzy *et al*., 1991; Bacry *et al*., 1993), used by Herrmann (1997, 1998), provides a more refined technique. It proceeds by tracking the lines of maximum modulus for varying resolution σ, and determining corresponding orders of singularity α (or γ, as in Section 2). This method allows for a direct estimation of local orders of singularity at those locations where a line of local maximum of the wavelet transform modulus can be identified.

3.1.1 Multifractal analysis of KTB neutron porosity log

To illustrate how the multifractality of a borehole log can be practically quantified, we provide here an example of a multifractal analysis using the KTB neutron porosity $\phi(z)$. These data consists of 19786 measurements at a depth interval of 0.152 m. Prior to analysis, we average these values over a bin size of 10 measurements to remove the inherent smoothing effect associated with the finite size of logging tool. Figures 6a and 6b show the KTB porosity log and its derivative. Figure 8b shows the power spectrum of $\phi(z)$, with a best-fit power law function: $E(k) \sim k^{-1.2}$, which corresponds with a Hurst exponent H=0.1 if $\phi(z)$ is modeled as a mono-scaling signal. Figure 8 also provides the scaling with ℓ of the moments of the increments of ϕ: $<|\delta\phi_\ell|^q> = <|\phi(z+\ell) - \phi(z)|^q>$ for q=1, 2, 3.

While the power law trend is clear for these moments, the fit is not fully satisfactory, perhaps due to the lack of data points. However, scaling of the power spectrum from the Nyquist scale up to ~1 km (at which point statistical convergence cannot be assumed) implies scaling of the moment of order q=2; we see that the departure from the power law fits is not severe and similar at different values of q. Plotting $<|\delta\phi_\ell|^q>$ versus $<|\delta\phi_\ell|^2>$ yields good power law trends, from which the structure function can be estimated. Direct estimation of $\zeta(q)$ from the scaling of $<|\delta\phi_\ell|^q>$ in $\sim \ell^{\zeta(q)}$ gives the structure function $\zeta(q)$ (Figure 8d), along with an estimate of the error on $\zeta(q)$ computed by varying the scaling interval of ℓ on which the scaling exponent is calculated. As the power law fit becomes less accurate at larger

q, the absolute error on $\zeta(q)$ increases. The clear non-linearity of $\zeta(q)$ indicates the multifractality of $\phi(z)$. A mono-scaling model of ϕ based on the Hurst exponent H=0.1 estimated from the power spectrum would yield a linear relationship $\zeta(q)$=0.1q.

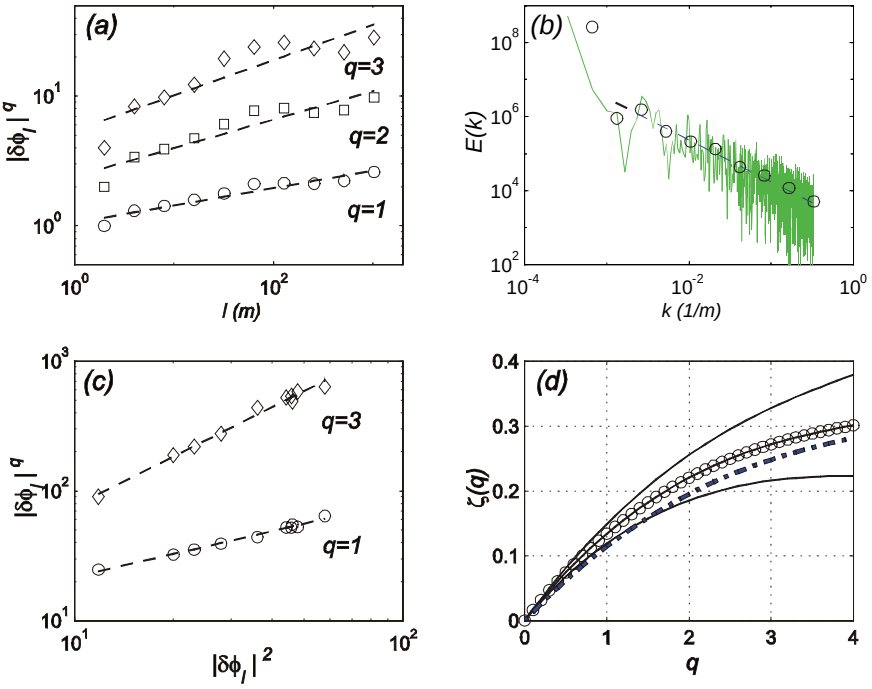

Figure 8. Multifractal analysis of the neutron porosity $\phi(z)$ of the KTB Main borehole (Figure 6). a) Scaling of the moments of order q=1, 2 and 3 of the increments $|\phi(z+\ell)-\phi(z)|$ with the scale ℓ in meters. b) Scaling of the power spectrum of ϕ, with the best power law fit in $E(k)\sim k^{-1.2}$ estimated by fitting $E(k)$ averaged over algebraically-spaced intervals (circles). c) Scaling of the moments of order 1 and 3 of the increments with the moment of order 2, allowing for a better constrained estimation of $\zeta(q)$ (see text for details). d) Structure function $\zeta(q)$ estimated: (circles) by direct fit of the scaling of the moments with scale ℓ (graph a), along with an estimate of the error (envelope in continuous lines), and (dot-dash) using the ESS method in c).

We have therefore demonstrated that there are significant variations in the local degree of variability for the KTB neutron porosity log. Bursts of rapid fluctuations are found along the borehole, showing that the variability is not homogeneously distributed. This intermittency is a fundamental feature of multifractal distributions.

Figures 6c and 6d display an example of a synthetic signal, along with its derivative, constructed with multi-scaling statistics close to those of the

actual KTB neutron porosity log. A fractional integration of a lognormal conservative multifractal was performed to obtain this synthetic signal.

Multifractal analysis and simulation can therefore be used for studying and simulating synthetic media with statistics that closely mimic those of the upper crust, and hence could improve our understanding of dynamical processes subjected to such heterogeneous conditions. We note that, for the upper crust, distinction between various multifractal models based on a numerical fit of the computed structure function of borehole logs is limited, given the large degree of uncertainty in the estimated $\zeta(q)$ (i.e., the error envelope on Figure 8d, obtained for the super-deep KTB borehole neutron porosity log, a signal already much longer than most other borehole logs). While there might exist a strong case in favor of log-infinitely divisible models, based on the $\lambda_1 \rightarrow 1$ limit discussed in Section 2.2, one cannot, with the presently available data, definitely decide on one model or the other. Hence we recommend using the simplest model that can reproduce the estimated $\zeta(q)$ within its error bars. Lognormal models are generally found to be of sufficient flexibility (by adjusting the curvature of the function, i.e., the relative value of the quadratic term in $\zeta(q)$) to yield such simple, acceptable models. A Matlab code for generating 1-D or 2-D lognormal conservative multifractals from continuous multiplicative cascades is given in the Appendix. Generalization to 3-D models is straightforward. However, the proposed 2-D (and 3-D) models are scalar models; the inclusion of principal directions (for example due to the presence of strong non-isotropic defects like faults) that can rotate with scale and position would require the development of non-scalar models.

3.2 Fractures and faults

The distribution of faults and fractures is commonly observed to be scale-invariant (e.g., see review of fracture experiments in Bouchaud, 1997). It has been proposed that scale-invariance of sonic logs could be due primarily to scale-invariant fracture distributions in the crust (e.g., Leary, 1991; Holliger, 1996; Leary, this volume), although lithologic variability is also likely to be important (e.g., Bean, 1996; Goff and Holliger, 1999; Marsan and Bean, 1999). In the crust, fractures are likely to be most important at shallow depths, where brittle fracturing is most intense, and that their role diminish at greater depths, where lithostatic pressure and emergence of the ductile regime tend to close them. If faults and fractures are indeed a primary source of heterogeneity in the upper crust, then their distribution at shallow depths would be of great importance for a variety of geophysical processes, such as scattering of seismic waves, fluid flow (seismically active faults are thought to be primary flow conduits; Barton *et al*., 1995), and faulting and

deformation processes. Here we review attempts at quantifying and understanding the multifractality of fracture and fault distributions and associated attributes (e.g., aperture, cumulative displacement).

Cowie *et al*. (1995) studied the scale-invariant statistics of a numerical model of elastic anti-plane deformation and faulting. Their original approach was to consider the temporal evolution of the deformation, showing that strain localization can be accurately measured by multifractal analysis. Deformation evolves from a nucleation regime, where small-scale fractures initiate randomly (due to quenched disorder), to a localized regime during which favored fractures grow, coalesce, and account for an always larger portion of the total deformation. This maturation is effectively quantified by looking at the development of multifractal statistics for the displacement field. As most of the cumulative displacement becomes localized on smaller and smaller domains (faults or clusters of faults), the heterogeneous character of the faulting process becomes more and more pronounced, resulting in spatially intermittent deformation.

An elegant attempt at analyzing the multifractality of observed fault distributions was presented by Ouillon and others (Ouillon *et al*., 1995; Ouillon and Sornette, 1996; Ouillon *et al*., 1996). Their approach was to compare multifractal scaling regimes, obtained by traditional box-counting methods, of a fault and fracture network map (in Saudi Arabia) from the 1 cm to the 100 km scale, with the associated global strike orientation regimes analyzed using an anisotropic wavelet transform analysis. Several regimes common to both analyses were detected that could correspond to characteristic scales in the crustal layering of the region. The main criticism that could be formulated here, and that would also apply to other studies on multifractal networks reviewed here, is that they ignore both the geometry and topology of a fault trace and the possibly scale-invariant statistics of fault orientation (strike), by applying an isotropic multifractal analysis that was originally developed for looking at heterogeneous sets of points (Poincaré sections of strange attractors). A step towards a more sophisticated and certainly more informative analysis would then be to use the wavelet transform used in the work by Ouillon and co-workers to give a density measure $\varepsilon(\underline{x},\ell,\theta)$ of how close we are, at location $\underline{x}$, from having a fault of size greater or equal to scale ℓ striking at θ. A full multifractal analysis could then be done on ε, taking the strike angle into consideration. Such a multifractal formalism still needs to be developed in the physics literature.

A very similar multifractal analysis was proposed by Weiss and Gay (1998) for the case of freshwater ice sample fracturing under uniaxial compression. Looking at the fracture networks developing at various stages during the test, weak multifractality was found, with two more or less mono-scaling competing regimes $N(\ell)\sim\ell^{-1}$ and $\sim\ell^{-2}$, where $N(\ell)$ is the number of

non-empty boxes at scale ℓ (boxes occupied by at least one fracture segment). At early stages in the fracturing, $N(\ell) \sim \ell^{-1}$ develops over more than two decades, then the second $\sim \ell^{-2}$ regime appears at large scale with a transition scale ℓ_c decreasing with time. The absence of multifractality before the onset of tertiary creep is expected to be due to the absence of strong pre-existing material heterogeneities, the samples being made from fresh water. In contrast to the model of Cowie *et al*. (1995), the authors only had access to the fracture network geometry, as opposed to a (scalar) displacement field. This precludes a full analysis of the localization of deformation leading to failure. The transition from one regime to the other is likely to be equivalent to the transition from a nucleation and growth stage of randomly distributed fractures (the topological dimension $D \approx 1$ for an individual fracture) to a coalescence regime, during which a dense (i.e., $D \approx 2$) percolating network of fractures is formed. During tertiary creep, localization of the deformation is observed with the development of a weak multifractal regime above the transition scale ℓ_c, demonstrating that the dynamical organization leading to the selection and growth of a macro fracture can be obtained even with very little initial disorder.

The simpler case of 1-D sections of fracture networks was studied by Belfield (1994). The scalar quantity was then the fracture apertures, and the data were collected from a microscanner probing horizontal boreholes. A direct multifractal box-counting analysis yielded good scaling fits of moments of various orders over more than two decades in scale, and revealed the clear multifractal character of those logs. A model, based on a multifractal strain distribution generated from a multiplicative cascade model was then proposed (Belfield, 1998) to explain and fit the analysis. (More precisely: from a micro-canonical, discrete (λ_1=2), 1-D cascade, with μ being defined as a (positive) Lévy law.) Note that such a cascade is not log-infinitely divisible, and would yield, in the limit of an infinite number of cascading steps, a lognormal cascade.

Finally, the multifractality of 1-D and 2-D mode-I fracture profiles was analyzed in Schmittbuhl *et al*. (1995). A clear departure of the structure function $\zeta(q)$ from linearity was found for the height of the fracture surface/cut. The implications of such a multifractality, which relates to the existence of heterogeneous distributions of asperities, are yet to be examined, especially in terms of contact, i.e., friction, properties of fractures and faults.

4. CONCLUSIONS

By fully accounting for the scaling variability present in the upper crust, as for example probed by borehole log measurements, multifractal modeling is particularly well-suited for characterizing small- and intermediate-scale crustal heterogeneity distributions. While the geophysicist involved in numerical/analytical modeling of dynamical processes taking place in such a variable environment can readily exploit the numerous attempts at analyzing and reproducing the statistics of the medium, several important issues still need to be addressed. For example, a full account of tensorial deformation in a multifractal medium is a particularly challenging problem. Multifractal modeling can also be used in order to account for the strong variability in seismicity distributions. A strongly heterogeneous brittle lithosphere can then be incorporated in dislocation models that systematically assume elastic homogeneity of the medium, and hence could reproduce the observed small-scale variability totally ignored in such models. The same can be said of poro-elastic models that typically assume normal (i.e., Brownian) fluid diffusion, hence an homogeneously permeable crust, while observations of fluid circulation in the crust (for example by looking at the water table level in wells) show how complex this process is.

ACKNOWLEDGMENTS

We would like to thank Agnès Helmstetter, François Schmitt, and Jérome Weiss, for their help in improving the clarity and quality of this paper, as well as Gareth O'Brien for testing the Matlab® code. Numerous comments by the reviewers helped the authors in focusing this manuscript. We also appreciated the patience of the editors John Goff and Klaus Holliger. The writing of this paper was initiated while D. M. was in receipt of an Enterprise Ireland postdoc fellowship.

APPENDIX

We propose in this appendix five Matlab® programs for the numerical simulation of lognormal multifractal (conservative and non-conservative) distributions, based on the various methods described in this paper.

```
function epsilon=lognormal_multifractal(Lambda,D,C1);
% EPSILON=LOGNORMAL_MULTIFRACTAL(LAMBDA,D,C1) generates
% a lognormal conservative multifractal EPSILON in D dimension, with scale ratio
% LAMBDA and a curvature of the moment scaling function K(q) equal
% to C1, i.e., K(q)=C1(q^2-q)
```

```
Lambda_D=1+(Lambda-1)*(D-1); gamma=randn(Lambda_D,Lambda);

Ktmp(1:Lambda/2+1)=(1:Lambda/2+1);
Ktmp(Lambda/2+2:Lambda)=Ktmp(Lambda/2:-1:2);
K=repmat(Ktmp,Lambda_D,1).^2; Kprime=K;
for a=1:D-1 Kprime=Kprime'; end;
K=sqrt(Kprime+K); ft_f=K.^(-D/2);

Gamma=real(ifft2(ft_f.*fft2(gamma)));
epsilon=exp(Gamma*sqrt(2*C1*log(Lambda)/mean(std(Gamma))^2));

function v=fractional(epsilon,chi);
% V=FRACTIONAL(EPSILON,CHI) performs a fractional integration (CHI>0)
% or derivation (CHI<0) of order CHI of EPSILON. This can be used to
% generate non-conservative multifractals, by fractionally integrating
% (CHI>0) conservative multifractals. EPSILON can be only 1-D or 2-D.

if(min(size(epsilon))==1) D=1; else D=2; end;
Lambda=max(size(epsilon)); Lambda_D=1+(Lambda-1)*(D-1);

Ktmp(1:Lambda/2+1)=(1:Lambda/2+1);
Ktmp(Lambda/2+2:Lambda)=Ktmp(Lambda/2:-1:2);
K=repmat(Ktmp,Lambda_D,1).^2; Kprime=K;
for a=1:D-1 Kprime=Kprime'; end;
K=sqrt(Kprime+K); ft_f=K.^(-chi);
v=real(ifft2(ft_f.*fft2(epsilon)));


function v=nonconservative_I(Lambda,C1,H);
% V=NONCONSERVATIVE_I(LAMBDA,C1,H) generates a 1-D non-conservative
% multifractal V of scale ratio LAMBDA, with a structure function
% zeta(q)=q*(H-C1*H)-(C1/H^2)*q^2, using the multifractal operational
% time method of Mandelbrot (1997). The parameter N gives the
% length of the fractional Brownian motion w, and can be modified.

N=2^18;
epsilon=lognormal_multifractal(Lambda,1,C1);
tau=cumsum(epsilon); tau=tau/max(tau)*N;

filter(1:N/2+1)=(1:N/2+1).^(-0.5-H); filter(N/2+2:N)=filter(N/2:-1:2);
w=real(ifft(fft(randn(N,1))'.*filter));
v=w(ceil(tau));

function v=nonconservative_II(Lambda,D,C1,chi);
% V=NONCONSERVATIVE_II(LAMBDA,D,C1,CHI) generates a non-conservative
% multifractal V of dimension D and scale ratio LAMBDA, and with a
% structure function zeta(q)=q*(CHI+C1)-C1*q^2, using the fractional
% integration method of Schertzer and Lovejoy (1987).
```

```
epsilon=lognormal_multifractal(Lambda,D,C1);
v=fractional(epsilon,chi);

function v=nonconservative_III(Lambda,C1,chi);
% V=NONCONSERVATIVE_III(LAMBDA,C1,CHI) generates a 1-D non-conservative
% multifractal V of scale ratio LAMBDA, with a structure function
% zeta(q)=q*(0.5+C1*0.5+CHI)-C1/4*q^2, using the two-step integration
% method of Marsan, Schmitt, and Bean (unpublished manuscript)
% NB: the spectral slope of V is beta=1+2*CHI

epsilon=lognormal_multifractal(2*Lambda,1,C1);
increment=epsilon.^(0.5).*randn(1,2*Lambda); w=cumsum(increment);
vlong=fractional(w,chi); v=vlong(Lambda/2+1:Lambda*3/2);
```

REFERENCES

Arneodo A., Grasseau, G., and Holschneider, M., 1988, Wavelet transform of multifractals, *Phys. Rev. Lett.* **61:**2281-2284.

Arneodo A., Bacry, E., and Muzy, J.-F., 1998, Random cascades on wavelet dyadic tress, *J. Math. Phys.* **39:**4142-4164.

Bacry E., Muzy, J.-F., and Arnéodo, A., 1993, Singularity spectrum of fractal signals from wavelet analysis: Exact results, *J. Phys. Stat.* **70:**635-674.

Barton C. A., Zoback, M. D., and Moos, D., 1995, Fluid flow along potentially active faults in crystalline rock, *Geology* **23:**683-686.

Bean C. J., 1996, On the cause of 1/*f*-power spectral scaling in borehole sonic logs, *Geophys. Res. Lett.* **23:**3119-3122.

Bean C. J., and McCloskey, J., 1993, Power-law random behaviour of seismic reflectivity in boreholes and its relationship to crustal deformation models, *Earth Plan. Sci. Lett.* **117:**423-429.

Belfield W. C., 1994, Multifractal characteristics of natural fracture apertures, *Geophys. Res. Lett.* **21:**2641-2644.

Belfield W. C., 1998, Incorporating spatial distribution into stochastic modelling of fractures: multifractals and Lévy-stable statistics, *J. Struct. Geol.* **20:**473-486.

Benzi R., Biferale, L., Crisanti, A., Paladin, G., Vergassola, M., and Vulpiani, S., 1993a, A random process for the construction of multiaffine fields, *Physica D* **65:**352-358.

Benzi R., Ciliberto, S., Baudet, C., Ruiz Chavarria, G., and Tripiccione, R., 1993b, Extended self-similarity in the dissipation range of fully developed turbulence, *Europhys. Lett.* **24:**275-279.

Bouchaud E., 1997, Scaling properties of cracks, *J. Phys. Cond. Mat.* **9:**4319-4344.

Cowie P. A., Sornette, D., and Vanneste, C., 1995, Multifractal scaling properties of a growing fault population, *Geophys. J. Int.* **122:**457-469.

Davis A., Marshak, A., and Wiscombe, W., 1994, Wavelet-based multifractal analysis of non-stationary and/or intermittent geophysical signals, in: *Wavelets in Geophysics* (E. Foufoula-Georgiou and P. Kumar, eds.), Academic Press, San Diego, pp. 249-298.

Dolan S. S., Bean, C. J., and Riollet, B., 1998, The broad-band fractal nature of heterogeneity in the upper crust from petrophysical logs, *Geophys. J. Int.* **132:**489-507.

Frisch, U., 1995, *Turbulence,* Cambridge University Press, Cambridge.

Goff J. A., and Holliger, K., 1999, Nature and origin of upper crustal seismic velocity fluctuations and associated scaling properties: Combined stochastic analyses of KTB velocity and lithology logs, *J. Geophys. Res.* **104:**13,169-13,182.

Grassberger P., and Procaccia, I., 1983, On the characterization of strange attractors, *Phys. Rev. Lett.* **50:**346.

Grecksch G., Roth, F., and Kümpel, H. J., 1999, Coseismic well-level changes due to the 1992 Roermond earthquake compared to static deformation of half-space solutions, *Geophys. J. Int.* **138:**470-478.

Halsey T. C., Jensen, M. H., Kadanoff, L. P., Procaccia, I., and Shraiman, B., 1986, Fractal measures and their singularities: the characterization of strange sets, *Phys. Rev. A* **33:**1141-1151.

Herrmann F. J., 1997, Multiscale analysis of well- and seismic data, PhD thesis, Delft University, Delft.

Herrmann F. J., 1998, Multiscale analysis of well- and seismic data, in: *Mathematical Methods in Geophysical Imaging V*, Proceedings of SPIE volume 3453 (S. Hassanzadeh, ed.), International Society for Optical Engineering, Belingham, Washington, pp. 180-208.

Herrmann H. J., and Roux, S., 1990, *Statistical Models for the Fracture of Disordered Media*, North-Holland, Amsterdam.

Holliger K., 1996, Fault scaling and 1/*f* noise scaling of seismic velocity fluctuations in the upper crystalline crust, *Geology* **24:**1103-1106.

Holliger, K., and Goff, J. A., A generic model for the 1/*f*-nature of seismic velocity fluctuations, this volume.

Holliger K., Green, A. G., and Juhlin, C., 1996, Stochastic analysis of sonic logs from the upper crystalline crust: Methodology, *Tectonophysics* **264:**341-356.

Huang Y., Saleur, H., Sammis, C., and Sornette, D., 1998, Precursors, aftershocks, criticality and self-organized criticality, *Europhys. Lett.* **41:**43-48.

Ito T., and Zoback, M. D., 2000, Fracture permeability and in situ stress to 7 km depth in the KTB scientific drillhole, *Geophys. Res. Lett.* **27:**1045-1048.

Leary P., 1991, Deep borehole log evidence for fractal distribution of fractures in crystalline rock, *Geophys. J. Int.* **107:**615-627.

Leary P. C., 1995, Quantifying crustal fracture heterogeneity by seismic scattering, *Geophys. J. Int.* **122:**125-142.

Leary, P. C., Fractures and physical heterogeneity in crustal rock, this volume.

Leonardi S., and Kümpel, H. J., 1999, Fractal variability in super deep borehole - implications for the signature of crustal heterogeneities, *Tectonophysics* **301:**173-181.

Liu H. H., and Molz, F. J. 1997, Multifractal analyses of hydraulic conductivity distributions, *Water Resour. Res.* **33:**2483-2488.

Lovejoy S., and Schertzer, D., 1985, Generalized scale invariance and fractal models of rain, *Water Resour. Res.* **21:**1233-1250.

Lovejoy S., Schertzer, D., and Tsonis, A. A., 1987, Functional box-counting and multiple elliptical dimensions in rain, *Science* **235:**1036-1038.

Lovejoy S., Pecknold, S., and Schertzer, D., 2001, Stratified multifractal magnetization and surface geomagnetic fields -I. Spectral analysis and modelling, *Geophys. J. Int.* **145:**112-126.

Main I. G., Peacock, S., and Meredith, P. G., 1990, Scattering attenuation amd the fractal geometry of fracture systems, *Pure Appl. Geophys.* **133:**283-304.

Mandelbrot B., 1974, Intermittent turbulence in self-similar cascades: divergence of high moments and dimension of the carrier, *J. Fluid Mech.* **62:**331-358.

Mandelbrot B., 1997, *Fractales, Hasard et Finance* (in French), Flammarion, France.

Mandelbrot B., and Van Ness, J. W., 1968, Fractional Brownian motions, fractional noises and applications, *SIAM Review* **10:**422-437.

Marsan D., and Bean, C. J., 1999, Multiscaling nature of sonic velocities and lithology in the upper crysalline crust: Evidence from the KTB Main Borehole, *Geophys. Res. Lett.* **26:**275-278.

Marsan D., Schertzer, D., and Lovejoy, S., 1996, Space-time multifractal processes: predictability and forecasting of rain fields, *J. Geophys. Res.* **101:**26,333-26,346.

Mehrabi A. R., Rassamdana, H., and Sahimi, M., 1997, Characterization of long-range correlations in complex distributions and profiles, *Phys. Rev. E* **56:**712-722.

Meneveau C., and Sreenivasan, K. R., 1987, Simple multifractal cascade model for fully developed turbulence, *Phys. Rev. Lett.* **59:**1424.

Muller J., 1992, Multifractal characterization of petrophysical data, *Physica A* **191:**284-288.

Muller J., 1993, Characterization of reservoir heterogeneities using multifractal statistics, *Ann. Geophys.* **11:**525-531.

Muzy J.-F., Bacry, E., and Arnéodo, A., 1991, Wavelets and multifractal formalism for singular signals: Application to turbulence data, *Phys. Rev. Lett.* **67:**3515-3518.

Nakao H., 2000, Multi-scaling properties of truncated Lévy flights, *Phys. Lett. A* **266:**282-289.

Newman W. I., Turcotte, D. L., and Gabrielov, A. M., 1995, Log-periodic behavior of a hierarchical failure model with applications to precursory seismic activation, *Phys. Rev. E* **52:**4827-4835.

Ouillon G., and Sornette, D., 1996, Unbiased multifractal analysis: Application to fault patterns, *Geophys. Res. Lett.* **23:**3409-3412.

Ouillon G., Sornette, D., and Castaing, C., 1995, Organisation of joints and faults form 1-cm to 100-km scales revealed by optimized anisotropic wavelet coefficient method and multifractal analysis, *Nonl. Proc. Geophys.* **2:**148-158.

Ouillon G., Castaing, C., and Sornette, D., 1996, Hierarchical geometry of faulting, *J. Geophys. Res.* **191:**5477-5487.

Painter, S., Statistical characterization of spatial variability in sedimentary rock, this volume.

Parisi G., and Frisch, U., 1985, A multifractal model of intermittency, in: *Turbulence and Predictability in Geophysical Fluid Dynamics and Climate Dynamics* (M. Ghil., R. Benzi, and G. Parisi, eds.), North-Holland, Amsterdam.

Pocheau A., 1998, Scale ratios, statistical symmetries and intermittency, *Europhys. Lett.* **43:**410-415.

Saucier A., and Muller, J., 1993, Use of multifractal analysis in the characterization of geological formations, *Fractals* **1:**617-628.

Saucier A., Huseby, O. K., and Muller, J., 1997, Electrical texture characterization of dipmeter microresistivity signals using multifractal analysis, *J. Geophys. Res.* **102:**10,327-10,337.

Schertzer D., and Lovejoy, S., 1987, Physical modeling and analysis of rain and clouds by anisotropic scaling multiplicative processes, *J. Geophys. Res.* **92:**9693-9714.

Schertzer D., Lovejoy, S., and Schmitt, F., 1995, Structures in turbulence and multifractal universality, in: *Small-Scale Structures in Three-Dimensional Hydrodynamic and Magnetohydrodynamic Turbulence* (M. Meneguzzi, A. Pouquet, and P. L. Sulem, eds.), Springer, Berlin, pp. 137-144.

Schertzer D., Lovejoy, S., Schmitt, F., Chigirinskaya, Y., and Marsan, D., 1997, Multifractal cascade dynamics and turbulent intermittency, *Fractals* **5:**427-471.

Schmitt F., and Marsan, D., 2001, Stochastic equations for continuous multiplicative cascades in turbulence, *Eur. Phys. J.* **20:**3-6.

Schmitt F., Schertzer, D., and Lovejoy, S., 1999,Multifractal analysis of foreign exchange data, *Appl. Stoch. Mod. Data Anal.* **15:**29-53.

Schmittbuhl J., Schmitt, F., and Scholz, C., 1995, Scaling invariance of crack surfaces, *J. Geophys. Res.* **100:**5953-5973.

Shamir G., and Zoback, M. D., 1992, Stress orientation profile to 3.5 km depth near the San Andreas fault at Cajon Pass, California, *J. Geophys. Res.* **97:**5059-5080.

She Z., and Leveque, E., 1994, Universal scaling laws in fully developed turbulence, *Phys. Rev. Lett.* **72:**336-339.

She Z., and Waymire, E., 1995, Quantized energy cascade and log-Poisson statistics in fully developed turbulence, *Phys. Rev. Lett.* **74:**262-265.

Sornette D., 2000, *Critical Phenomena in Natural Sciences*, Springer, Berlin.

Sornette D., and Sammis, C., 1995, Complex critical exponents for renormalization group theory of earthquakes: Implications for earthquake prediction, *J. Phys. I* **5:**607-619.

Taqqu M., 1987, Random processes with long-range dependence and high variability, *J. Geophys. Res.* **92:**9683-9686.

Todoeschuck J. P., Jensen, O. G., and Labonte, S., 1990, Gaussian scaling noise model of seismic reflection sequences: Evidence from well logs, *Geophysics* **55:**480-484.

Vicsek T., and Barabasi, A.-L., 1991, Multi-affine model for the velocity distribution in fully turbulent flows, *J. Phys. A* **24:**L845-L851.

Weiss J., and Gay, M., 1998, Fracturing of ice under compressional creep as revealed by a multifractal analysis, *J. Geophys. Res.* **103:**24,005-24,016.

Wu R. S., Xu, Z., and Li, X. P., 1994, Heterogeneity spectrum and scale-anisotropy in the upper crust revealed by the German Continental Deep-Drilling (KTB) Holes, *Geophys. Res. Lett.* **21:**911-914.

Yaglom A. M., 1966, The influence of the fluctuation in energy dissipation on the shape of turbulent characteristics in the inertial range, *Sov. Phys. Dokl.* **2:**26-29.